Ocean Engineering 349 (2026) 123886

Contents lists available at ScienceDirect

Ocean Engineering

journal homepage: www.elsevier.com/locate/oceaneng

A composite modelling approach for the fatigue analysis of offshore wind turbines considering corrosion-induced material degradation

James McAuliffe, Brian Broderick, Breiffni Fitzgerald *

Department of Civil, Structural and Environmental Engineering, School of Engineering, Trinity College, Dublin, Ireland

ARTICLE INFO

Keywords:
Fatigue analysis
Offshore wind turbines
Multibody dynamics
Finite element modelling
Stress concentration factors (SCFs)

ABSTRACT

Accurate fatigue damage prediction is essential for the safe and cost-effective design of offshore wind turbines. However, the large scale and offshore deployment of modern turbines poses significant challenges for accurately modelling their long-term behaviour. This work proposes a composite modelling framework combining a non-linear multibody dynamic (MBD) model and a high-fidelity finite element (FE) model to improve fatigue life predictions. It represents the first fatigue assessment of the IEA 15-MW reference wind turbine tower and explicitly considers a newly designed bolted ring flange connection at the tower base. The MBD model, with 22 degrees of freedom, accurately captures the system-level response of the turbine under operational wind and wave loading. However, it cannot resolve local stresses at fatigue-critical details. To address this, stress concentration factors (SCFs) derived from a FE model are used to enhance the MBD-derived stress histories. The composite modelling framework is applied to a known fatigue hotspot, specifically the butt weld at the tower base which connects the tower shell to a specifically designed ring flange connection. The inclusion of SCFs arising due to the presence of the bolted ring flange act to reduce the predicted fatigue life by 19.3 %, demonstrating the substantial influence of stresses induced by local geometric features on fatigue performance. The study additionally considers time-varying SCFs resulting from corrosion-induced material loss. Employing time varying SCFs and assuming a five-year effective corrosion protection period, the predicted fatigue life decreases to 13.39 years, failing to achieve the desired 20-year design life. These results demonstrate the critical importance of incorporating the effects of both local geometry and corrosion into fatigue assessments of offshore wind turbines.

1. Introduction

Over the past two decades, wind turbines have dramatically increased in both size and capacity as the industry strives to maximise energy capture and position wind energy as a viable competitor to conventional fossil fuel-based generation. The development of offshore wind turbines has enabled access to the rich aeolian resources of the open sea, where higher wind speeds and improved airflow quality enhance power production. However, the increased scale and offshore location of modern, multi-megawatt wind turbines introduce complex structural and operational challenges. The growing length of turbine blades and corresponding tower heights have led to increasingly slender and flexible structures. These large-scale systems experience highly dynamic responses under the elevated aerodynamic and hydrodynamic loads characteristic of offshore environments. The rotating mass of the turbine blades, in an atmospheric boundary layer characterised by wind shear, further contributes to the operational demands of these systems, imposing substantial cyclic, gravitational forces on key structural components. Consequently, modern offshore wind turbines are subjected to intensified cyclic loading, often exceeding 10 million load cycles over a 20-year design life (Kensche, 2006), while operating in the corrosive conditions of the marine environment. The combination of these factors makes wind turbines and their components highly susceptible to fatigue damage, directly impacting their operational lifespan. Accurate fatigue assessments are therefore fundamental to ensuring structural integrity, optimising structural steel requirements, planning maintenance strategies (Lotsberg, 2025), and assessing life extension opportunities in offshore wind turbines.

Accurately assessing the accumulation of fatigue damage under the stochastic conditions experienced by wind turbines requires simulation methodologies capable of effectively capturing the dynamic response of the system. A key computational approach for simulating the behaviour of wind turbines is multibody dynamics. This approach is central to state-of-the-art wind turbine simulation tools such as OpenFAST (Jonkman et al., 2024), Bladed (DNV, 2022), and HAWC2 (Larsen and Hansen, 2007), which leverage MBD principles to capture the intricate

* Corresponding author.
E-mail address: breiffni.fitzgerald@tcd.ie (B. Fitzgerald).

https://doi.org/10.1016/j.oceaneng.2025.123886
Received 18 July 2025; Received in revised form 19 November 2025; Accepted 2 December 2025
Available online 6 January 2026

interactions among aerodynamic and hydrodynamic forces, structural flexibility and control systems. Given that fatigue assessments rely on stress time histories derived from realistic, time-varying operational scenarios, MBD simulations are particularly well-suited for this task. Consequently, MBD models have been widely adopted in fatigue research to evaluate the long-term structural performance of wind turbines (Saenz-Aguirre et al., 2022; Sørum et al., 2022; Wang et al., 2022; Song et al., 2023; Tao et al., 2024; Li et al., 2024; Pu et al., 2025). These papers collectively demonstrate the capability of MBD models to accurately and efficiently simulate the global response of wind turbine structures under a wide range of environmental and operational conditions. However, stemming from their reliance on simplified representations of complex geometries, MBD models often lack the granularity required to precisely predict the true stresses experienced by specific detailed components of the turbine, such as bolts, welds, or flanges. To achieve this level of detail, high-fidelity structural modelling approaches, such as FE analysis, are essential.

Finite element analysis enables the development of high-fidelity models that facilitate detailed examination of individual wind turbine components, allowing for the accurate evaluation of local stresses and strains. Finite element analysis has been extensively applied in both the frequency and time domains for fatigue analysis of wind turbines (Stavridou et al., 2015; Hu et al., 2016; Zhang et al., 2018; Sajeer et al., 2020; Boudounit et al., 2023; Li et al., 2023; Peng et al., 2023). However, the finite element method (FEM) suffers from a number of limitations when performing fatigue analysis. Frequency-domain methods are limited in their ability to accurately model nonlinear effects inherent in wind turbine dynamics (Zhang et al., 2024b), while performing simulations in the time domain gives rise to substantial computational expenses. A further constraint arises from the inability of conventional FE software to compute aerodynamic loads directly, presenting a significant limitation for wind turbine analysis given their exposure to large, stochastic wind fields. Without integrated aerodynamic calculations, FE simulations must rely on simplified load inputs or externally derived aerodynamic solutions such as Hsu et al. (2014), Muskulus and Schafhirt (2015), Yang et al. (2015), Huo and Tong (2020). However, such integrated models often decouple structural responses from aerodynamic load calculations, while also giving rise to large computational expenses. As a result, significant simplifications are often required to make simulations feasible within practical timeframes. These compromises, while necessary, can limit the accuracy of the stress predictions. To retain the high fidelity provided by FE models without incurring excessive computational costs, an effective strategy is to apply SCFs in combination with computationally efficient dynamic simulations.

SCFs serve as a bridge between local and global structural assessments, providing a means to account for the effects of macro geometry on stress distributions (Radaj et al., 2006). The use of SCFs allows lower-fidelity FE models to be employed in fatigue analysis by enabling local stresses to be estimated from global structural responses. This approach significantly reduces computational cost while maintaining accuracy and has become widely adopted in FE-based fatigue assessments of offshore structures (Dong et al., 2011, 2012; Yeter et al., 2014b,a, 2016; Zwick and Muskulus, 2016; Lotsberg, 2016; Hegseth et al., 2021; Chen et al., 2022). However, as with general FE models, many of these approaches struggle to accurately capture the complex loading conditions experienced by wind turbines. To address this, lower-fidelity FE models incorporating SCFs have been integrated with MBD models (Do et al., 2015; Ren et al., 2023). This coupling enables the simulation of the turbine's holistic response to environmental loading, including aerodynamic, hydrodynamic, and control system interactions, while still allowing for the accurate estimation of local stresses in critical components. Although the use of SCFs allows for reduced-fidelity FE models to be employed, these approaches remain constrained by the computational demands associated with the dynamic FE simulations, often necessitating significant simplifications within the FE model.

To bypass the requirement of dynamic FE simulations while still capturing accurate local stress responses, researchers have coupled MBD models with SCFs derived from empirical/analytical formulas, or extracted from high-fidelity FE analyses. This approach enables efficient fatigue assessment without compromising the accuracy of local stress predictions. Several recent studies have highlighted the effectiveness and versatility of this method for fatigue life estimation. Velarde et al. (2020) applied this methodology in a fatigue analysis, which assessed the fatigue design factors assigned in the DVN-GL standard. The time domain simulations were performed using HAWC2 based on the DTU 10-MW offshore wind turbine (Bak et al., 2013) and the stresses were computed considering a SCF of 1.1 at a welded connection at the base of the turbine tower. The study concluded that a fatigue design factor of at least 3 should be recommended by standards. Fu et al. (2020) emphasised the critical role of localised stress analysis in their investigation of the fatigue damage in wind turbine tower flanges and bolts. Fatigue loads in the connection flange and bolts at the turbine tower base were calculated using the rainflow counting algorithm and Palmgren-Miner's rule with a SCF of 1.12 applied to the stress histories for the connection flange. The study concluded that fatigue failure in the flange would occur significantly earlier than in any of the bolts. Nispel et al. (2021) adopted the methodology to investigate the effect of soil-structure interaction on the fatigue life of NREL's 5-MW offshore wind turbine employing nonlinear springs at the mudline. Fatigue damage over a 30-year design life at a site in Blyth, UK, was estimated using the rainflow counting algorithm and Palmgren-Miner's rule, incorporating a SCF and a bi-linear S–N curve from the DNV standard. The analysis identified wind loading as a key contributor to fatigue damage, while other parameters such as tower stiffness and material properties were found to have reduced influences. Zhu et al. (2023) applied the coupled approach while additionally accounting for the influence of corrosion on the turbine tower. The fatigue damage was calculated using the rainflow counting algorithm and Palmgren-Miner damage rule, incorporating an S-N curve for seawater with cathodic protection provided by the DNV standard. To account for local effects, stresses obtained from OpenFAST simulations were adjusted using SCFs and a thickness correction factor. The study concluded that in the absence of additional inspections and maintenance in corrosive environments, the failure probability increases approximately tenfold over a period of 10 service years.

This finding underscores the significant impact of corrosion on the structural reliability of offshore wind turbines. Corrosion-related damage has been identified as a contributing factor in approximately 8 % of all offshore structural failures (Adasooriya et al., 2020). This concern is especially relevant as modern wind turbines are increasingly deployed in aggressive offshore environments, where regions experiencing high SCFs are also subjected to elevated corrosion rates. Despite this, the time-dependent effects of corrosion are often overlooked in current design standards (Adasooriya et al., 2017). An effective strategy to address this limitation is to account for material degradation over time directly into SCF calculations, thereby allowing more realistic fatigue life assessments of offshore structural components considering the effects of corrosion-induced material thinning. Dong et al. (2012) explored this approach performing a fatigue analysis considering the effects of corrosion on the welded connections of a jacket-type offshore wind turbine support structure using Efthymiou's formulas (Efthymiou, 1988) to calculate the hotspot stresses. The study found that if no maintenance is carried out following the failure of the protection system, the probability of failure of the support structure increases significantly. Li et al. (2022) similarly implemented the Efthymiou empirical formula to calculate SCFs in the tubular joints of a monopile-based tripod substructure. This paper found that the reduced thickness of joints caused by corrosion resulted in a significant decrease in the fatigue capabilities of the support structure. Extending the effects of corrosion thinning to a global scale, Okenyi et al. (2023) performed a stress analysis of the IEA 15-MW offshore wind turbine subjected to corrosion via Euler-Bernoulli beam theory and FEA. The results of the two analyses showed good agreement, illustrating the increase in stresses observed in the turbine support structure and tower that arise due to the corrosion. The paper demonstrated the importance of considering material wastage due to corrosion in stress analysis to provide safe and accurate designs. Taking a more detailed approach at the component level, Zhang et al. (2024a) proposed a probabilistic Corrosion-Fatigue (C-F) deterioration model for high-strength bolts of wind turbine flange connections. The study found that, due to the combined effects of corrosion and fatigue, the bolts' service life could be reduced to as little as 30.4 % of their original expected life span. The significant reductions in life span reported in these papers make corrosion-induced degradation a critical aspect which must be considered in fatigue analysis to ensure accurate lifespan predictions for systems operating in corrosive environments, such as offshore wind turbines.

In this study, a fatigue analysis of the IEA 15-MW monopile-based offshore wind turbine is conducted using a proposed composite model framework. This framework is created through one-way coupling, integrating SCFs derived by a FE model with stresses time histories computed by a MBD model. Within the composite modelling framework, a MBD model is developed capable of accurately capturing the wind turbine's operational response to both aerodynamic and hydrodynamic loading in an efficient manner. However, this model considers the turbine's structural components at a system level, relying on generalised mass and stiffness distributions, which do not take into consideration the influences of local geometry changes, flanges, welds, access doors, platforms, etc. To accurately capture the stress concentrations which arise from such discontinuities, a detailed FE model of the wind turbine is constructed, detailing accurate geometric and material properties of the wind turbine.

The fully constructed composite model is applied to evaluate the fatigue performance of the IEA 15-MW wind turbine, presenting the first fatigue assessment of this monopile-based wind turbine tower. This analysis explicitly accounts for the influence of a specifically designed bolted ring flange connection at the tower base, an important factor that has often been neglected in the literature. A key enhancement of this study is the incorporation of material thinning in fatigue-prone regions, through the parametric capabilities of the FE model. By integrating corrosion wastage effects into the fatigue assessment, the composite modelling framework provides a realistic assessment of the turbine's fatigue life and structural performance under real-world operating conditions. The developed model is applied to a representative site off the east coast of the United States, establishing a benchmark fatigue performance evaluation under typical met-ocean conditions.

A preliminary version of this work was presented in McAuliffe et al. (2024), where an initial corrosion-fatigue assessment was carried out using a simplified approach for calculating stresses at the tower–flange connection. The present study extends and improves upon that earlier work in several important ways. First, a newly designed ring flange connection has been developed and evaluated under the greatly increased suite of IEC design load cases, resulting in a more realistic and robust flange design. Second, the finite element model incorporating this connection has been refined to provide stress calculations with improved accuracy. Third, the method for deriving SCFs has been revised to follow a more widely adopted and standardised approach. Finally, the focus of the fatigue analysis has shifted from the flange connection itself to the butt weld connecting the ring flange to the tower shell, a recognised fatigue-critical detail.

To provide an understanding of the distinct roles and capabilities of the modelling approaches employed within the composite model, Section 2 provides a detailed discussion of the framework, beginning with an overview of the MBD and FE modelling strategies and their respective contributions to the composite model. Section 3 outlines the calculation of the SCFs considering the effects of corrosion thinning. Section 4 describes the fatigue analysis methodology employed to estimate the lifespan of the butt weld component. Section 5 presents and compares the results of fatigue analysis obtained from the composite modelling approach and the traditional modelling strategy. Finally, Section 6 provides concluding remarks and discusses the implications of the findings for future design and assessment practices.

Table 1
IEA 15-MW specifications (Gaertner et al., 2020b).

Parameter	Value
Turbine class	IEC Class 1B
Specific rating	332 W/m^2
Rotor diameter	240 m
Hub height	150 m
Blade length	117 m
Root diameter	5.2 m
Max chord	5.77 m
Tip prebend	4 m
Precone	4Â°
Cut-in wind speed	3 m/s
Rated wind speed	10.59 m/s
Cut-out wind speed	25 m/s
Design tip-speed ratio	90
Minimum rotor speed	5 rpm
Maximum rotor speed	7.56 rpm
Maximum tip speed	95 m/s
Design tip-speed ratio	9
Drivetrain	Direct drive
Shaft tilt angle	6Â°
Transition piece height	15 m
Monopile embedment depth	45 m
Monopile base diameter	10 m

2. Methodology

2.0.1. Details of the IEA 15-MW wind turbine

The composite model is constructed based on the IEA 15-MW offshore reference wind turbine. The design and specifications of this state-of-the-art wind turbine were released by the IEA in association with NREL (Gaertner et al., 2020b) to act as a benchmark model within the research community. The key specifications of the turbine, as outlined by the IEA, are provided in Table 1.

2.1. Composite modelling framework

The composite model developed in this work is designed to integrate the strengths of both the MBD and FE models, addressing the individual limitations of each while maximising their combined effectiveness. By combining the MBD model's efficient and holistic system-level dynamic response capabilities with the FE model's precision in simulating local stresses, the composite model aims to deliver accurate results for critical wind turbine components at a reduced computational cost. The overall structure of this composite modelling framework is illustrated in Fig. 2. Within this framework, the FE model is utilised to calculate SCFs at geometric discontinuities in fatigue-prone regions of the wind turbine support structure. Simultaneously, the nonlinear aeroelastic MBD model captures the holistic response of the wind turbine, generating stress time histories for a range of environmental conditions based on the turbine's operational state. Post-processing these results, the composite model produces localised stress time histories which are then used to estimate the fatigue life of the component. To implement this framework, both an MBD model and a detailed FE model of the IEA 15-MW wind turbine were developed. The FE model developed explicitly incorporates a custom-designed ring flange connection, allowing its influence on fatigue performance to be evaluated within the composite model framework.

2.2. Multibody dynamic model

The nonlinear aeroelastic MBD model is employed to capture the operational dynamic response of the wind turbine under environmental

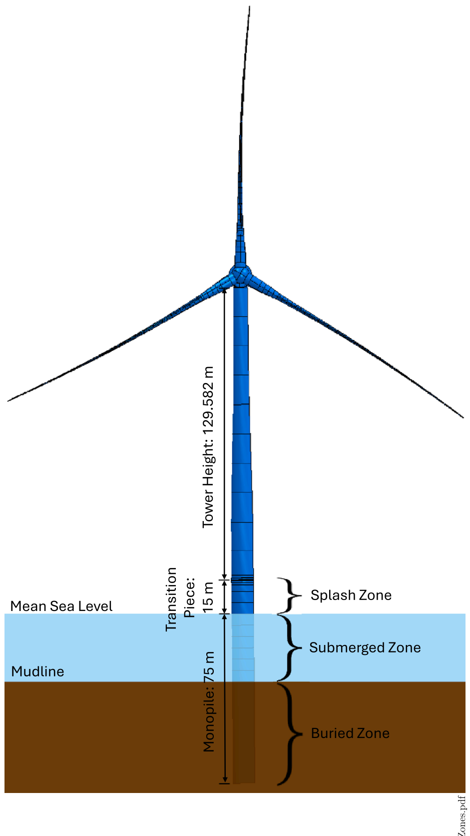

Fig. 1. Corrosion zone classification for the 15-MW finite element model.

loading. In this study, the model is specifically employed to calculate the axial forces and bending moments occurring at the connection between the turbine tower and the transition piece. The model is formulated using Kane's Dynamics (Kane and Levinson, 1985), which offers computational efficiency for systems with highly coupled dynamic behaviour. The model incorporates 22 Degrees Of Freedom (DOFs) to capture the motion of both rigid and flexible components of the turbine. For this model, the tower is defined to include the transition piece and the portion of the monopile above the mudline while the remainder of the monopile is modelled as a rigid body characterised by six DOFs, three translational (q_{Sg}, q_{Sw}, q_{Hv}) and three rotational (q_R, q_P, q_Y). The deformation response of the turbine tower is modelled with four DOFs, based on the first two mode shapes in both the side-to-side (q_{TSS1}, q_{TSS2}) and fore-aft (q_{TFA1}, q_{TFA2}) directions. These modes capture the dominant dynamics of the tower, while axial and torsional deformations are neglected. Due to the rigid nature of the turbine hub and nacelle, only two DOFs are required to describe their motion. The rotation of the rotor nacelle assembly about the longitudinal axis of the turbine tower, enabling the turbine to align with the wind direction, is described as the nacelle yaw motion q_{yaw}. Additionally, the rotational position of the hub/rotor blades is assigned as the generator azimuth q_{GeAz} or rotor angle. The torsion of the low-speed shaft is considered using one DOF q_{DrTr}, with its flexibility modelled using a spring-damper system. Finally, the elastic deflections of the three blades are represented by nine DOFs. Each blade's elastic response is described based on the first and second flapwise mode shapes (q_{BiF1}, q_{BiF2}) and the first edgewise mode shape (q_{BiE1}) where i represents the blade number.

In this work, a fixed-base condition is applied at the mudline, constraining these six DOFs and effectively neglecting soil-structure interaction. While this assumption generalises the system and reduces the computational complexity, it also introduces limitations by neglecting the flexibility and damping effects of the surrounding soil. By introducing the fixed-base constraint, the monopile behaves as a perfectly rigid foundation, resulting in an artificially stiffer system with higher natural frequencies compared to a more realistic flexible foundation. Additionally, by neglecting the soil structure interaction, the energy dissipation through both material and radiation damping of the surrounding soil mass is disregarded in the model. These effects influence the dynamics of the turbine, reducing the accuracy of the predicted structural response.

Kane's method was selected for its vector-based formulation, which provides a systematic and efficient way to derive the equations of motion for MBD systems. Stemming from Newton's laws of motion, the generalised equilibrium equations for a simple holonomic multi-body system, can be expressed as:

$$F_r + F_r^* = 0 \qquad \text{for } r = 1, 2, \dots\ N \tag{1}$$

where N denotes the total number of DOFs in the system.

The term F_r is known as the generalised active force corresponding to the r^{th} DOF of the system. It is determined for a set of n rigid bodies, each defined by a reference frame N_i and centre of mass point X_i, using the following expression:

$$F_r = \sum_{i=1}^{n} \left[{}^{E}\mathbf{v}_r^{X_i} \cdot \mathbf{F}^{X_i} + {}^{E}\boldsymbol{\omega}_r^{N_i} \cdot \mathbf{M}^{N_i} \right] \tag{2}$$

$\mathbf{F}^{X_i}$ is the force vector acting on the centre of mass of point X_i and $\mathbf{M}^{N_i}$ is the moment vector acting on the N_i rigid body. The terms ${}^{E}\mathbf{v}_r^{X_i}$ and ${}^{E}\boldsymbol{\omega}_r^{N_i}$ represent the partial linear and partial angular velocity of the point X_i and rigid body N_i respectively associated with the r^{th} DOF in the inertial (E) reference frame. The generalised inertia force corresponding to the r^{th} DOF is given as:

$$F_r^* = -\sum_{i=1}^{n} \left[{}^{E}\mathbf{v}_r^{X_i} \cdot \left(m^{N_i}\, {}^{E}\mathbf{a}^{X_i} \right) + {}^{E}\boldsymbol{\omega}_r^{N_i} \cdot {}^{E}\dot{\mathbf{H}}^{N_i} \right] \tag{3}$$

where it is assumed that the inertia forces for each rigid body N_i are applied at its centre of mass point, denoted as X_i. The term ${}^{E}\dot{\mathbf{H}}^{N_i}$ refers to the time derivative of the angular momentum of the rigid body N_i around its centre of mass X_i within the inertial reference frame E. Further details regarding these general equations are outlined by Kane and Levinson in their seminal work on dynamics Kane and Levinson (1985).

By taking the time derivatives of the system's generalised coordinates, the partial linear and angular velocities of key points and rigid bodies can be determined. These velocities are then used to formulate the complete non-linear time-domain equations of motion for the fixed-base wind turbine, expressed in their general form as:

$$\mathbf{M}(\mathbf{q}, \mathbf{u}, t)\ddot{\mathbf{q}} = -\mathbf{f}(\dot{\mathbf{q}}, \mathbf{q}, \mathbf{u}, t) \tag{4}$$

Here, $\mathbf{M}$ represents the inertial mass matrix, which is a non-linear function of the system's DOFs $\mathbf{q}$, control inputs $\mathbf{u}$, and time t. The force vector $\mathbf{f}$ similarly depends non-linearly on the DOFs, control input and time in addition to the time derivative of the DOFs. The numerical simulations performed in this work were conducted using MATLAB (2018), solving the non-linear system of equations with a time step of 0.005 seconds using the Runge-Kutta 4th order method, commonly referred to as 'ODE 4'.

Many of the system's active forces are time-dependent and influenced by the dynamic behaviour of the system's components. To accurately capture these complex interactions, the MBD model is developed using a modular framework. In this approach, individual modules are designed to handle specific mathematical calculations which can then be interconnected, enabling full coupling of the global system. The hydrodynamics module is used to model the sea conditions experienced by the wind turbine based on the Pierson–Moskowitz spectrum (Pierson and Moskowitz, 1964), which characterises sea states by the significant wave height and peak spectral period. This module employs the Airy wave theory to account for wave and current interactions, allowing for two-dimensional flow to be considered. The hydrodynamic forces acting on the monopile and tower are estimated using Morison's equation

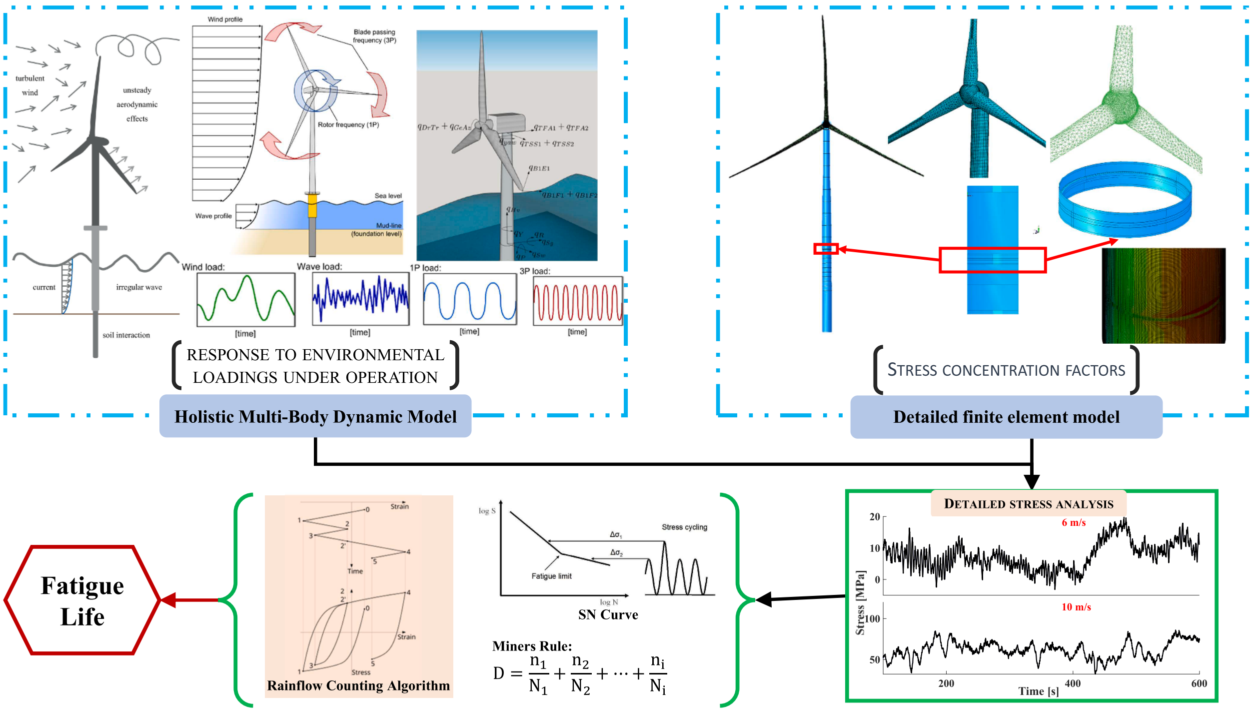

Fig. 2. Composite modelling framework flowchart.

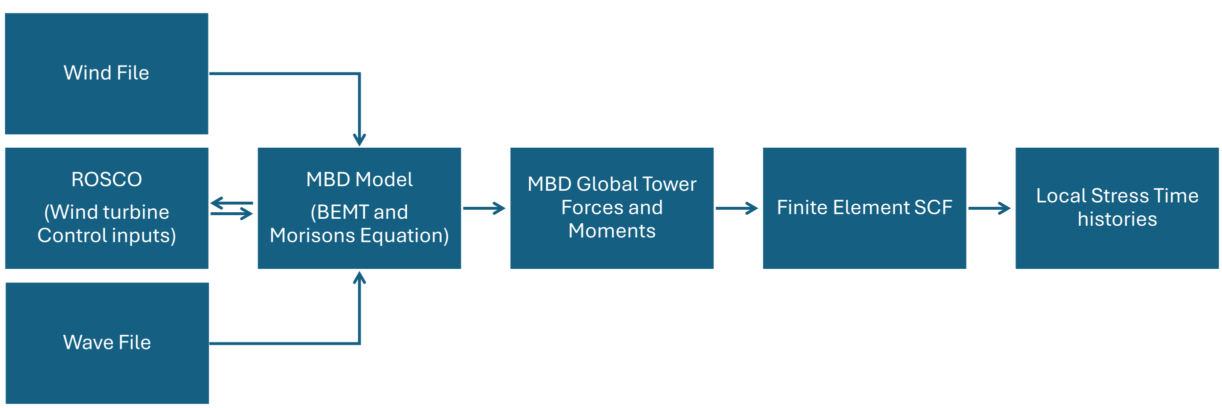

Fig. 3. Signal pathway from aerodynamic/hydrodynamic loading to tower stress histories.

(Morison et al., 1950), combined with strip theory. The aerodynamic loads on the turbine blades are calculated using Blade Element Momentum (BEM) theory implementing wind profiles generated via TurbSim (Jonkman, 2009). The blade pitch angle is updated at each time step using NREL's Reference OpenSource Controller (ROSCO) with rate limits, saturation constraints, and yaw misalignment explicitly modelled in line with OpenFAST defaults. Further details of the controller architecture and implementation are available in Abbas et al. (2021).

The signal path from global loads produced by the MBD model to local stresses is explicitly captured in Fig. 3. In this framework, the tower base axial forces and bending moments obtained from the MBD simulation are combined with FE-derived SCFs to generate local stress time histories. This path ensures that the structural response reflects control-mediated aerodynamic and hydrodynamic loading, thereby enabling for accurate fatigue assessment.

The MBD model, incorporating these calculations within its modular framework, has been rigorously validated through a code-to-code comparison with the state-of-the-art wind turbine simulator OpenFAST (Jonkman and Buhl, 2005), provided by NREL. This validation demonstrated strong agreement between the models, with detailed results outlined in Baisthakur and Fitzgerald (2025) and Baisthakur and Fitzgerald (2024). For a comprehensive understanding of the derivations of the formulas implemented in this MBD model, readers are referred to Sarkar and Fitzgerald (2021), while additional details on the modelling can be found in Sarkar et al. (2020), Sarkar and Fitzgerald (2020).

2.3. Ring flange connection design

The specifications of the 15-MW reference wind turbine are detailed in the IEA Wind TCP Task 37 technical report (Gaertner et al., 2020b), with additional supporting data files available on GitHub. While these resources provide a comprehensive overview of the turbine's design, the reports lack specific details regarding connection types, locations and dimensions within the support structure's components. To address this limitation, a connection between the tower base and the transition piece was designed in order to evaluate its influence on the fatigue damage experienced by the wind turbine tower. The connection is assumed to be a bolted ring flange connection, which is the most commonly

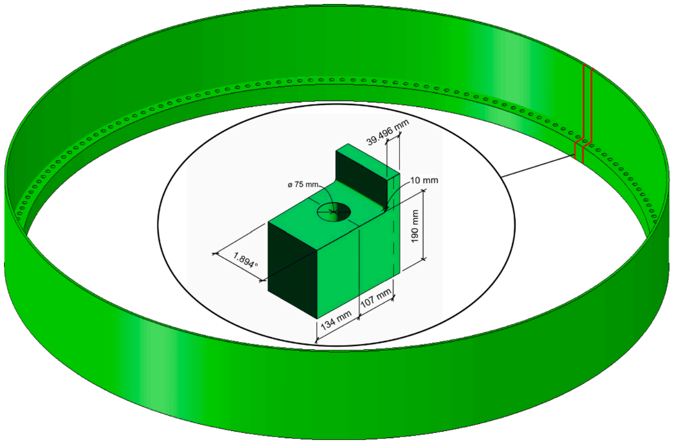

Fig. 4. Ring flange connection dimensions.

employed design for joining wind turbine tower segments and substructures (Weijtjens et al., 2021). The custom ring flange connection was designed using elastic-plastic theory, based on the ultimate limit state of the connection, following the Petersen/Seidel approach as outlined in IEC 61400-6 (International Electrotechnical Commission, 2020). The flange was designed to withstand the maximum loads encountered during Damage Load Cases (DLC) 1.3, 1.4, 1.5, 2.3, 3.2, 3.3, 4.1, 4.2, 6.2, 6.3, and 7.1. As dipiected in Fig. 4, the flange has a thickness of 190 mm and is fastened with 190 M72 bolts made of 10.9-grade high-strength steel. The modelling of the bolts is considered beyond the scope of this study, therefore the two flange components were connected using fixed constraints, assuming full surface contact between the mating faces.

2.4. Finite element model

A three-dimensional FE model of the IEA 15-MW monopile-based offshore wind turbine was developed using Abaqus/CAE software (Abaqus, 2011), with a particular emphasis placed on accurately calculating the SCFs that arise in the tower wall above the proposed ring flange connection. The model was built using a parametric modelling approach, implemented via a custom Abaqus–MATLAB interface to enable automated and flexible model generation. This approach allowed for the automation of model generation and facilitated the efficient adjustment of key geometric and material properties.

The detailed FE model incorporates geometric components supplied by the IEA, which have been adapted for use in Abaqus, along with additional parts derived from IEA data files (Gaertner et al., 2020b). The high-fidelity model includes intricate components such as the wind turbine blades, yaw mechanism, bearings and flanges. The geometric and material properties as defined in Gaertner et al. (2020a) were utilised in creating the FE model, providing a structurally precise depiction of the turbine. For the support structure, the transition piece and monopile components are represented as a single component in the FE model, consistent with the IEA geometry and data files. At the top of this component, corresponding to the transition piece, the internally bolted ring flange connects it to the base of the turbine tower. The modelling of the flange bolts is considered outside the scope of this work, and the two flanges are connected using a tie constraint, assuming full surface contact between the mating flanges. As the flanges are positioned at the top of the transition piece and at the base of the tower, as depicted in Fig. 4, the respective components are shortened by the thickness of the flange, ensuring that a tower top height of 144.582m is maintained. A fixed boundary condition was applied at the mudline of the monopile, located 30m below Mean Sea Level (MSL), thus neglecting soil-structure interactions. Given that this boundary condition is located over 45m from the ring flange connection, it has a negligible influence on the stresses at the flange which are governed primarily by the local geometry and material behaviour. The wind turbine was modelled in a parked configuration, with the yaw system aligned upwind. The rotor was held stationary, and the blades were restricted from pitching, maintaining a feathered position throughout the simulations.

To minimise computational cost, the nacelle elements including the yaw mechanism, the bedplate, the nacelle flanges, the low-speed shaft, the low-speed shaft bearings, the rotor, the stator and the hub were modelled as rigid components consistent with the approach used in the MBD model. The remaining components including the blades, the tower, the monopile/transition piece and the internally bolted ring flange connections, were modelled as deformable finite elements.

2.4.1. Element selection

The rigid components housed within the nacelle in addition to the hub were meshed using hexahedral elements of type C3D8R, selected for their low computational cost. The flexible blade components were meshed using C3D10. These quadratic tetrahedron elements were selected for use due to their high geometric versatility, which was required to accurately capture the intricate geometry of the turbine blades. In the case of the turbine tower and monopile/transition piece, conventional shell elements were used based on a reference surface generated from IEA specifications with the thickness of the components specified using sectional properties. In a similar manner to Hu et al. (2014), the shell element selected was the S4R element. The internal ring flange components and tower/transition piece elements within 1m of the flange component were meshed using C3D20R elements a general-purpose nonlinear element. This element was selected as when provided with a relatively fine mesh, this element is capable of modelling accurate stress concentrations as required in this work.

2.4.2. Local seeding and mesh convergence

Local seeding was implemented to minimise the computational cost of the FE model while maximising the accuracy of the results. By applying local seeding within the model, the computational efforts could be focused on the flange connection, ensuring efficient use of computational resources and maintaining high-resolution in this key area of interest. The local seeding strategy imposed divided the turbine into four regions, as depicted in Fig. 5.

- Region 1: This region consists of the flange connection and wall elements up to a height of 1m above the flange top surface. This region includes the flanges at both locations, at the base of the turbine tower and at the top of the monopile/transition piece. This particular region is selected as the key findings from the model are obtained from this section, and thus, the accuracy of stresses in this area are prioritised.
- Region 2: This region contains the upper and lower sections of the tower and transition piece, excluding region 1. These regions act as transition zones in both the tower and monopile. A further subdivision within the regions is made at a distance of 2m from the flange, with 1m belonging to Region 1. Within this 2m distance, the elements are meshed with the same seed length as Region 1. Outside of this distance, the elements transition gradually to the coarser mesh of Region 3 using a single bias.
- Region 3: This region includes all of the remaining segments of the tower and monopile components.
- Region 4: This region encompasses all of the other components, including the rotor nacelle assembly and the wind turbine blades.

Based on the local seeding strategy, a mesh convergence study was conducted to determine an appropriate seed length for each region of the turbine components. The mesh convergence aimed to maximise the accuracy of the stresses induced while minimising the computational expense for the total model. The mesh convergence analysis was performed by implementing a static analysis with a bending moment applied at the top of the turbine tower while observing the maximum axial stress experienced in the turbine tower flange connection (Region 1).

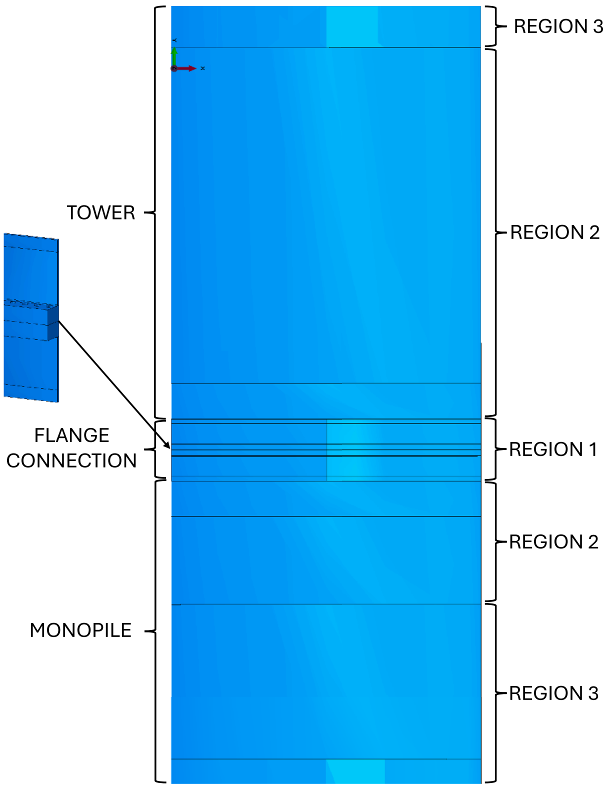

Fig. 5. Finite element model mesh regions.

Region 4, including the blade, hub, and nacelle components, being of secondary interest for this study, in which the stresses are not of great concern was meshed with a maximum seed size of 1m or with the maximum seed size that the software allowed for each component. To determine appropriate seed lengths for Regions 1, 2, and 3, a two-step mesh convergence study was conducted. In the first step, mesh convergence was performed for Region 1, while a fine mesh was applied in Region 3. An optimal seed length of 0.0197m was identified for Region 1, as shown in Fig. 6, resulting in a mesh with over 1.4 million elements. The seed size corresponds to half the tower wall thickness, and thus complies with the DNV guidelines, which recommend a maximum seed length of 50 % of the component thickness to ensure a minimum of two elements across the depth. By implementing such a resolution, stress gradients arising across the wall thickness can be captured effectively.

After selecting a suitable seed length for Region 1, a further mesh convergence was implemented on Region 3, with Region 2 being adjusted accordingly to comply with Region 1 and 3 seed lengths. The seed lengths in these regions had minimal influence on the resulting flange stress. Consequently, a seed length of 0.6m was selected for Region 3, minimising computational demands. By applying this local seeding strategy, the corresponding FE model was constructed, comprising of 1,440,800 elements, balancing computational cost and solution accuracy.

2.4.3. *Validation of finite element model*

To verify the accuracy and reliability of the FE model, a modal analysis was conducted to determine the natural frequencies and the corresponding mode shapes of the turbine tower for comparison against the benchmark values provided by the IEA. For the reference model without the flange connection, the fundamental side-to-side natural frequency was identified as 0.17008 Hz, closely matching the IEA-specified value of 0.17 Hz. This represents a deviation of less than 0.05 %, indicating excellent agreement. Further confidence in the FE model was established by examining the mode shape corresponding to the first natural frequency in the side-to-side direction depicted in Fig. 7. The close agreement between the FE model predictions and the IEA-specified values demonstrates the validity of the modelling approach and the fidelity of the developed FE model, establishing confidence in the use of the FE model for subsequent analyses.

3. Stress concentration factor calculation

Once the FE model was finalised, the SCF at the butt weld connection between the turbine tower and ring flange were calculated. This SCF is utilised with the nominal stresses produced using the MBD model to calculate local stresses surrounding the flange connection. There are two main components which contribute to the stress concentration at this location, the geometry effect of the ring flange and the notch effect stemming from the butt weld itself. The stress concentration arising from the notch effect is considered in the S-N curves provided by the DNV recommended practice guidelines (DNV, 2019) which are utilised in this fatigue analysis. As a result, the FE model does not consider any notch effects and solely focuses on the SCF arising from the geometric discontinuity of the ring flange.

Geometric SCFs can be calculated using several approaches, in this work, an approach described in Peterson's book (Pilkey et al., 2020) was adopted. In this approach, the geometric stress is calculated using a model with a geometric discontinuity present and is compared with the nominal stress calculated in an identical model without the discontinuity. In the case of this particular study, the structural discontinuity is the ring flange connection, thus, two models of the turbine are compared, one with the flange connection and the reference model without the connection. Using the FE model, the nominal and local peak stresses are calculated based on an idealised structure with no fabrication or installation misalignments and all material behaviour considered linear as specified by the DNV GL recommended practice guidelines (DNV, 2019). There are no existing guidelines on the recommended location of butt welds in the current literature or design standards, as a result in this paper the butt weld is selected to be located in the most onerous location along the tower wall in a bid to explore the worst case scenario.

The DNV recommended practice standard (DNV, 2019) states that for structures which are subject to several types of loading, in this case, axial forces and bending moments, the SCFs can be calculated for each loading scenario individually and later superimposed on the individual stresses. Consequently, two calculations are required for this work. The axial SCFs are found by applying an axial load of 10,000 kN at the turbine tower top and comparing the stresses calculated in the reference model against the stress produced in the model with the proposed flange. The bending moment SCFs are calculated in a simialr manner, placing a concentrated moment of 100,000 kNm at the top of the turbine tower.

To validate the SCFs calculated along the tower wall using the FE model, an analytical approach proposed by Seidel (2020) is employed. The resulting SCF distribution is directly compared to that obtained from the FE model under identical loading conditions, as presented in Fig. 8. The analytical solution exhibits behaviour consistent to that observed in the FE model, with both distributions following comparable trends along the length of the tower wall. However, the analytical equation tends to overestimate the bending stresses induced by the presence of the flange in comparison with the FE model. Despite these minor discrepancies, the overall close agreement between the two results reinforces confidence in the accuracy of the FE model's stress predictions.

3.1. *Corrosion induced degradation*

A novel aspect of this study lies in the FE model's capability to simulate the effect of corrosion on the turbine structure once corrosion protection measures are deemed to have failed. This is achieved by examining the effective thinning of the turbine tower. The corrosion effects are incorporated by simulating material wastage over time, leveraging the

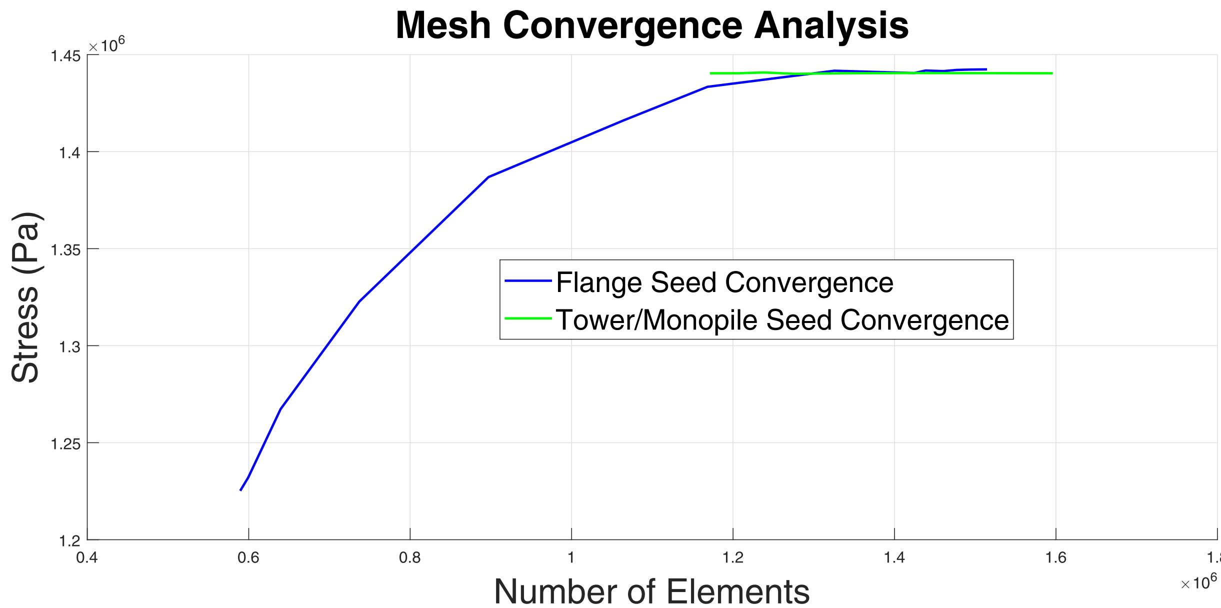

Fig. 6. Mesh convergence analysis.

parametric design of the turbine tower, ring flange, and monopile/transition piece to reduce the thickness of the components within the FE model. This material wastage reduces the effective area of the component, which gives rise to increased stresses and consequently causes the SCFs to vary with time. This time-varying SCF methodology is consistent with the approach of Li et al. (2022), who applied empirical formulae to capture corrosion effects.

As corrosion protection measures are only expected to remain effective for a limited number of years (Adasooriya et al., 2020) and with the repair of such coatings proving to be a difficult procedure in offshore conditions, the analysis is carried out considering a number of durations for which the corrosion protection is expected to remain effective. Upon failure of the corrosion protection coatings, the conventional approach of uniform corrosion is adopted. The rate at which the corrosion occurs is based on the exposure of the individual element. Specifically, a thinning rate of 0.1 mm/year for uncoated carbon steel is applied to the substructure in the atmospheric, submerged, and buried zones while a corrosion thinning rate of 0.3 mm/year is applied in the splash zone in accordance with ISO 19,920 (Petroleum, 2007) and IEC 61,400 (International Electrotechnical Commission, 2019). The corrosion zones, as illustrated in Fig. 1, were defined in this study as per Okenyi et al. (2023), which implemented the DNVGL-RP-0416 guidance (DNV, 2016) for the IEA 15-MW wind turbine.

3.2. Stress calculation

The MBD model is used to generate corresponding time histories of the axial forces and bending moments experienced at the tower base. The shear forces at the tower base are neglected as the resulting shear stresses are significantly lower than those arising from the axial and bending stress (Zhu et al., 2023). Additionally, across the full range of environmental conditions, the axial forces exhibited minimal variation over time and were, therefore considered to be constant. Therefore using the axial forces and bending moments with the time-varying SCFs, stress time histories for each simulation can be calculated for each individual year using Eq. (5).

$$\sigma_{E,i}(t) = SCF_{Axial\_i} \cdot \frac{-N}{A} + SCF_{Bending\_i} \cdot \frac{M_{FA}(t)\cos(\theta)}{Z} + SCF_{Bending\_i} \cdot \frac{M_{SS}(t)\sin(\theta)}{Z} \tag{5}$$

In this equation, $\sigma_{E,i}$ is the stress at the tower base at a time t during simulations conducted under environmental conditions E, subjected to i years of corrosion wastage. SCF_{Axial_i} and $SCF_{Bending\_i}$ are the axial and bending SCFs for each year considering the effects of the corrosion wastage, N is the axial force, A is the area of the tower cross-section, M_{FA} and M_{SS} are the bending moments in the fore-aft and side-to-side directions and θ represents the angle of the resultant moment vector relative to the fore-aft direction, given by:

$$\theta = \tan^{-1}\left(\frac{M_{SS}(t)}{M_{FA}(t)}\right) \tag{6}$$

The section modulus Z is derived from the second moment of area I for a hollow circular cross-section:

$$Z = \frac{D_{\text{outer}}}{2I}, \qquad I = \frac{\pi\left(D_{\text{outer}}^4 - D_{\text{inner}}^4\right)}{64} \tag{7}$$

Here, D_{outer} and D_{inner} are the outer and inner diameters of the tower cross-section, respectively. This formulation calculates the maximum stress observed at the tower base at any given time. As the magnitudes of the fore-aft and side-to-side moments vary over time, the location of the maximum stress correspondingly changes. To adopt a conservative assessment, the maximum stress values calculated throughout the duration of the time history are applied to a single location.

4. Fatigue analysis approach

4.1. Environmental conditions

The met-ocean conditions were selected based on data provided by NREL for a site on the east coast of the United States (Stewart et al., 2016) with all wind and wave loadings assumed to be fully aligned. The simulations were performed for IEC Design Load Case (DLC) 1.2 exclusively, while other load cases, such as DLCs 2.4, 3.1, 4.1, and 6.4 were neglected. DLC 1.2 represents typical power production conditions for the wind turbine for which a normal turbulence model can be assumed. This focus on DLC 1.2 is justified, as Huo and Tong (2020) indicate that 99.5 % of the total fatigue damage in wind turbines occurs during operational conditions.

For DLC 1.2, environmental conditions are selected based on discrete wind speeds, which are subsequently paired with suitable ocean

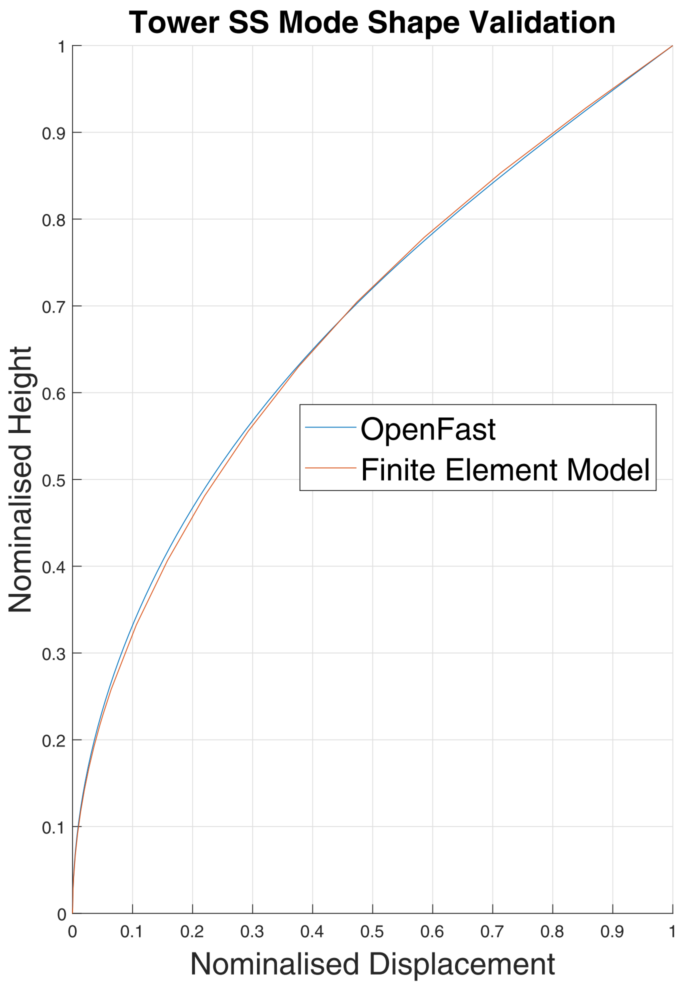

Fig. 7. Tower fundamental mode shape (side-to-side).

conditions. The environmental data was provided at a wind speed resolution of 2 m/s. For each wind speed, met-ocean parameters were defined, including significant wave height and peak spectral wave period, to comprehensively characterise the environmental conditions at the site. In line with IEC 61400-1 (International Electrotechnical Commission, 2019), at least six 10-minute simulations of usable simulation data for each environmental condition are required. Consequently, each simulation in this study was conducted for a duration of 675 seconds, with the initial 75 seconds discarded in order to eliminate the effects of the initial transient phase. To facilitate reproducibility and enable consistent comparisons under these environmental conditions, NREL provided six randomised turbulence seeds alongside the detailed environmental parameters. These random seeds were implemented as inputs into the Turbsim software (Jonkman, 2009) to generate the 3-D wind fields.

The probability distribution of the environmental conditions was modelled based on the wind speeds using a two-parameter Weibull distribution, with a shape factor of 2.12 and a scale factor of 9.767. Turbulence intensity data corresponding to the wind speeds was not provided. To address this, a turbulence model proposed by Wang et al. (2014) and recommended by the IEC (International Electrotechnical Commission, 2014) was employed to establish a relationship between wind speed and turbulence intensity. A site of class A was selected to provide conservative results for this model, reflecting higher turbulence conditions.

The post-processing of the simulation results was conducted using a modified version of NREL's software package, MLife (Hayman and Buhl, 2012). MLife performs short-term fatigue analysis by processing the time histories of each set of wind speeds coupled with their corresponding wave conditions. To calculate short-term fatigue, MLife employs Palmgren-Miner's rule combined with the Goodman correction, in conjunction with the rainflow counting algorithm as specified in Annex G of IEC 61400-1 (International Electrotechnical Commission, 2019). For each environmental condition, the six random seeds are evaluated to determine the total fatigue damage accumulated over the 3600 (6x600) seconds. To extend the short-term fatigue results into long-term fatigue results, the short-term fatigue damage values are integrated using the estimated frequencies to find the long-term damage accumulated. This analysis was applied on an annual basis calculating the accumulated fatigue damage at the turbine tower connection butt weld for an individual year. Following the concept of partial damage encapsulated in Palmgren-Miner's rule, the fatigue damage incurred in each year is added sequentially and the component is considered to have failed when the cumulative damage reaches unity.

The key modification made to MLife in this work involved adding the ability to perform fatigue analysis using bi-linear S-N curves. Given that the turbine tower sections are assumed to be prefabricated in an off-site manufacturing facility, the welding procedure is assumed to be performed in the flat position. Consequently, the DNV recommended practice standard class D S-N curves (DNV, 2019) can be implemented for the butt weld connecting the tower shell and flange connection. In this work, both the S-N curves for steel exposed to seawater with cathodic protection and steel exposed to seawater with free corrosion were applied depending on the status of the corrosion protection measure at the time in question. As these S-N curves are constructed based on a reference plate with a thickness of 25 mm, a thickness correction factor must be applied via a modification of the stress range.

5. Results

5.1. Modal analysis

The impact of material wastage due to corrosion on the dominant first natural frequency of the turbine tower was investigated through modal analysis. The evolution of the side-to-side natural frequency of the wind turbine tower as it undergoes material wastage due to corrosion is presented in Table 2. The table provides the natural frequency values and the percentage change relative to the initial condition at installation. The models used in this comparison include the ring flange connection to ensure consistency throughout.

Considering that corrosion protection measures in the splash zone will typically have a life span of up to 5 years (Momber, 2016), the analysis indicates that over the standard 20-year life span of a wind turbine, the natural frequency of the tower is reduced by 1.66 %. This relatively small change illustrates that corrosion wastage has a negligible impact on the natural frequency of the turbine, particularly when compared to potential frequency shifts caused by alternative influences such as soil-structure interaction (Fitzgerald and Basu, 2016).

5.2. Stress concentration factors

While its impact on global dynamics is minimal, corrosion is shown to have a significant effect on local SCFs. Table 3 presents the maximum SCF occurring along the shell wall near the flange connection when independently subjected to axial forces and bending moments. These values correspond to the first 50 years of service, during which corrosion protection is assumed to have failed, initiating corrosion wastage.

The stress distribution patterns associated with these maximum SCFs are illustrated in Figs. 9 and 10. These figures illustrate the SCF patterns for both axial and bending loads highlighting the significant impact of corrosion wastage on SCF values.

In these figures, the stress distribution pattern for the first year is represented by the bottom plot, with each subsequent year corresponding to the next plot above it. The variation of the SCFs over time follows a polynomial trend, highlighting the increasing impact of corrosion wastage

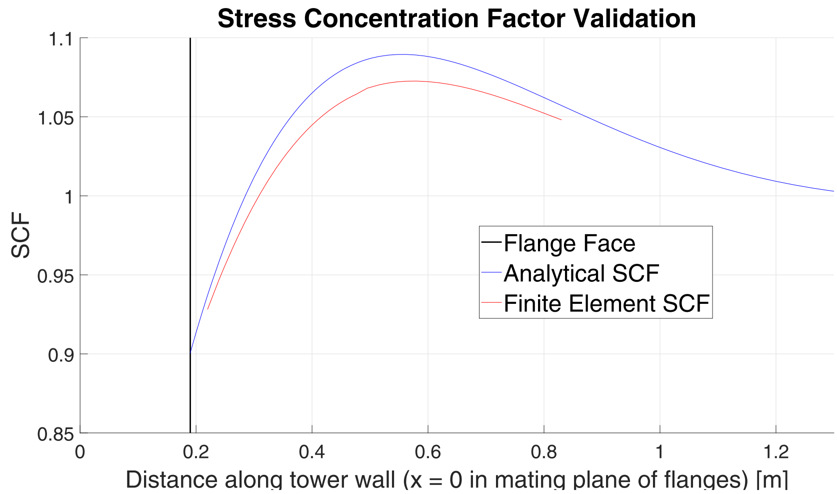

Fig. 8. SCF distribution Finite element model vs analytical approach.

Table 2
Variation in side-to-side natural frequency (%).

Corrosion Exposure (Years)	0	5	10	15	20	30	40	50
Natural Frequency (Hz)	0.170	0.169	0.168	0.167	0.166	0.164	0.161	0.158
Natural Frequency shift (%)	–	0.45	1.05	1.66	2.32	3.71	5.30	7.09

Table 3
Axial and bending SCF values in tower shell for years 1–50.

Year	Axial SCF	Bending SCF	Year	Axial SCF	Bending SCF
1	1.0663	1.0632	26	1.3207	1.3170
2	1.0747	1.0717	27	1.3337	1.3300
3	1.0830	1.0798	28	1.3469	1.3432
4	1.0915	1.0883	29	1.3600	1.3563
5	1.1002	1.0970	30	1.3732	1.3695
6	1.1091	1.1060	31	1.3873	1.3835
7	1.1182	1.1149	32	1.4011	1.3975
8	1.1273	1.1240	33	1.4154	1.4118
9	1.1366	1.1332	34	1.4301	1.4265
10	1.1461	1.1427	35	1.4451	1.4415
11	1.1553	1.1518	36	1.4599	1.4562
12	1.1654	1.1619	37	1.4756	1.4721
13	1.1753	1.1719	38	1.4913	1.4878
14	1.1854	1.1819	39	1.5076	1.5043
15	1.1954	1.1920	40	1.5246	1.5211
16	1.2056	1.2021	41	1.5415	1.5380
17	1.2163	1.2128	42	1.5592	1.5557
18	1.2272	1.2237	43	1.5762	1.5730
19	1.2383	1.2347	44	1.5947	1.5915
20	1.2495	1.2458	45	1.6127	1.6096
21	1.2606	1.2570	46	1.6317	1.6286
22	1.2723	1.2688	47	1.6510	1.6481
23	1.2840	1.2803	48	1.6712	1.6683
24	1.2959	1.2924	49	1.6915	1.6887
25	1.3079	1.3044	50	1.7121	1.7095

throughout the wind turbine's lifespan. This relationship indicates that as material degradation progresses, the rate at which the SCFs increase accelerates, leading to more pronounced stress concentrations.

5.3. Fatigue life evaluation

Table 4 presents the estimated fatigue life of the butt weld connection between the wind turbine tower and the transition piece assuming that the corrosion protective system remains fully functional for the full service life of the turbine. In this table, the fatigue life of wind turbine is calculated based on the traditional approach, where the flange connection is neglected and the composite model approach, which accounts localised stresses induced by the presence of the flange. The analysis yielded a fatigue damage rate of 0.0318 per annum when employing the traditional approach and 0.0407 per annum employing the composite model.

Table 4
Fatigue life.

	Traditional Approach	Composite Model
Lifespan (Years)	31.45	24.57

This significant decrease in the lifespan of the turbine tower is a direct consequence of stress concentration at the ring flange and highlights the importance of accounting for stress concentrations in the fatigue analysis framework. The SCFs calculated for both the axial and bending stresses act to increase the local stresses by approximately $\approx 7\%$. This translates into a $\approx 14\,\%$ increase in the amplitude of the stress cycle ranges which are incorporated into the bi-linear S–N curve. As the slope of the S–N curve in the high-cycle region is steep ($m = 5$ for corrosion protection and $m = 3$ for free corrosion), increases in stress ranges can lead to large reductions in fatigue life. As a result, the bending-induced stress amplification at the ring flange accelerates local fatigue damage accumulation. This increase in the stresses results in a 19.3 % reduction of the expected lifespan of the wind turbine, demonstrating the sensitivity of the fatigue life to the localised stress effects.

Considering that corrosion protection measures employed in the splash zones of wind turbines often rapidly degrade and become ineffective (Adasooriya et al., 2020), the fatigue analysis was extended to consider varying durations of corrosion protection effectiveness. Table 5 evaluates five levels of corrosion protection, corresponding to durations of 0, 5, 10, 15, and 20 years of intact protection. During these periods, no material wastage is assumed, and the S-N curve for steel exposed to seawater with cathodic protection is applied. After the assumed protection period, the protection is taken to have completely failed, exposing the structure to free corrosion. It is noted that in practice, offshore towers are protected through combined coating and cathodic protection systems that are actively managed via scheduled inspections, monitoring, and possible recoating or repair. Accordingly, the results presented in this study should be interpreted as bounding scenarios designed to as-

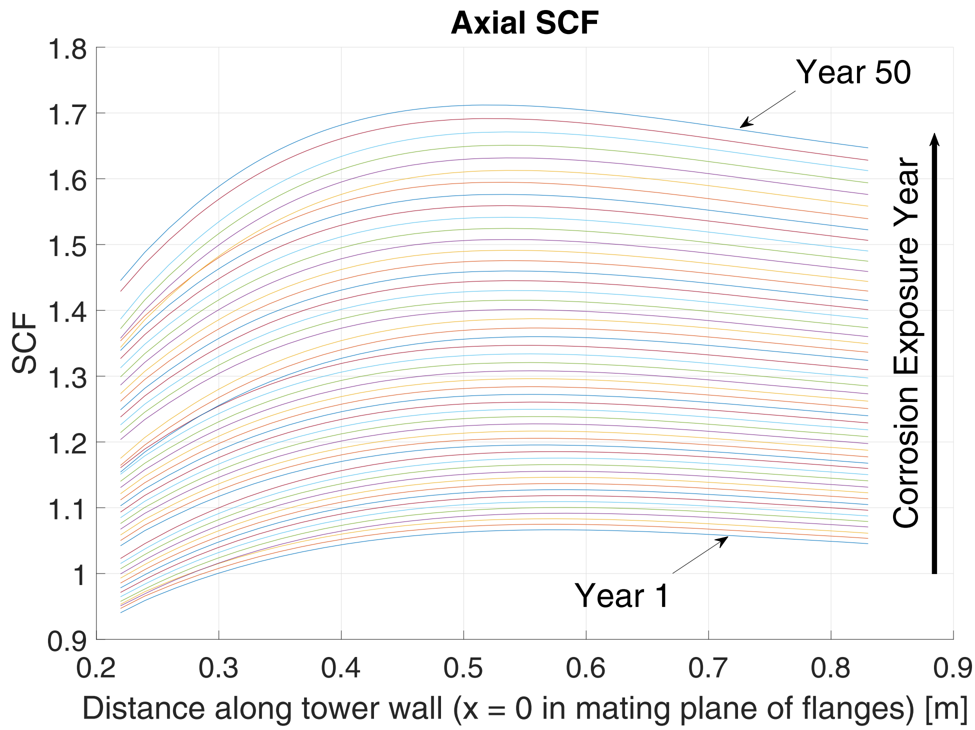

Fig. 9. Axial SCF distribution evolution over 50 years of corrosion exposure.

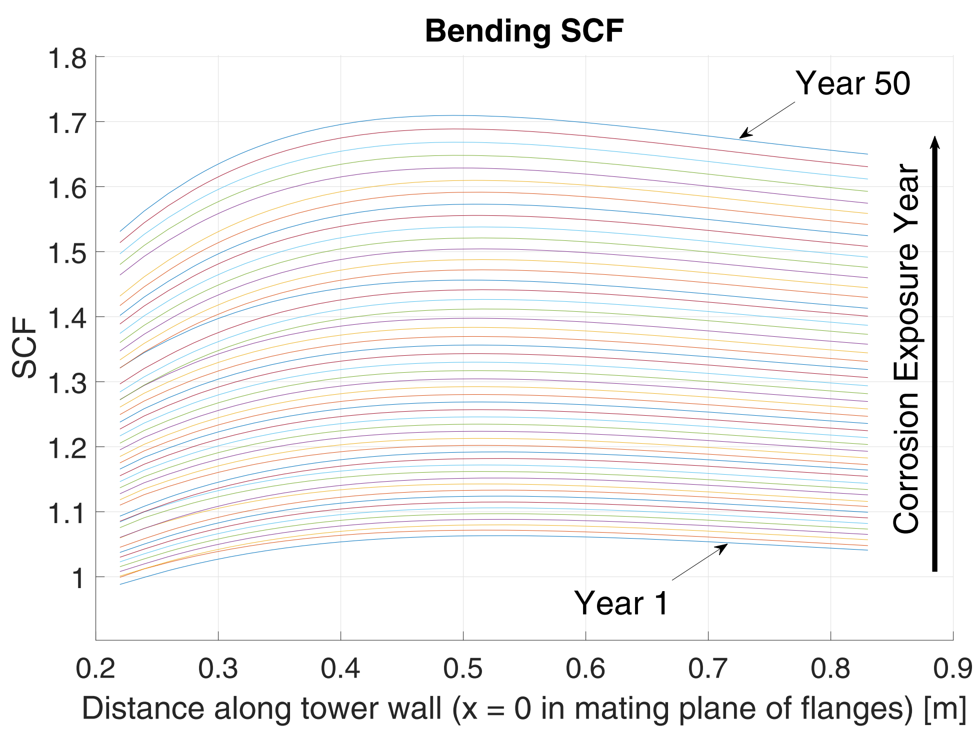

Fig. 10. Bending SCF distribution evolution over 50 years of corrosion exposure.

sess sensitivity to protection loss, rather than as direct simulations of site-specific maintenance plans. Within this context and considering the limited lifespan of corrosion protection measures in the splash zone, the most realistic scenarios are represented by the 0 and 5-year protection durations (Momber, 2016).

Table 5 highlights the critical impact of corrosion on lifetime estimation. The fatigue life neglecting such effects is found in Table 4 to be 24.57 years. However, under free corrosion conditions, where no protective measures are considered, the fatigue life is significantly

Table 5
NREL conditions: tower life span.

Years protection	20	15	10	5	0
Estimated Life Span (Years)	22.08	19.27	16.37	13.39	10.50

reduced to 10.5 years. This represents a 57 % reduction in fatigue life, leading to a lifespan of just over half of the desired 20-year service life. Implementing a typical corrosion protection system that remains effective for the first five years of the service life extends the fatigue life by 2.89 years, reducing the overall fatigue life reduction to 45 %. With each additional five years of effective protection, the fatigue life increases by an average of 2.9 years, clearly demonstrating the benefits of corrosion mitigation. Nonetheless, to avoid failure and keep cumulative fatigue damage within the acceptable limits over the full 20-year period, the welded component would require at least 16.29 years of effective corrosion protection.

6. Conclusion

This work presents a composite modelling approach to calculate the expected fatigue life of a butt weld on an internally bolted ring flange connection used to join the tower base and transition piece of in a 15-MW offshore wind turbine. The composite model integrates the capabilities of both multibody dynamic model simulations and finite element analysis, leveraging the strengths of both methods. This integrated approach enables accurate fatigue life assessments of critical wind turbine components, ensuring improved predictions of operational lifespan.

Within this composite model, a fully coupled 22 DOF aero-hydro-servo-elastic MBD model is used to simulate environmental loading conditions, calculating nominal stress time histories at the base of the wind turbine tower. These stress time histories are applied with SCFs calculated from a FE model of the turbine, which accurately account for the effects of local geometries. This enables the framework to simultaneously account for both global system dynamics and local stress distributions.

A novelty of this work arises in the ability of the FE model to update the SCFs of the fatigue-prone areas over time as corrosion-induced wastage alters the substructure's geometry, thereby inducing a global redistribution of stresses. Using these time varying SCFs, the composite model can produce the time histories of the local stresses occurring in the tower base considering the effects of material thinning of the components. Based on these stress time histories which vary annually, the fatigue life of the butt weld can be estimated using a modified version of NREL's MLife incorporating bi-linear S-N curves specified by DNV guidelines.

To validate the use of time-varying SCFs with the MBD model simulations, this study investigated the influence of corrosion thinning on the natural frequency of the wind turbine tower. The modal analysis conducted concluded that material wastage has a negligible effect on the natural frequency of the turbine tower, enabling a single set of dynamic simulations to remain applicable and accurate across the 50-year service life assessed in this study.

Once validated, a fatigue analysis was carried out employing comprehensive stress-time histories considering environmental conditions based on NREL's west coast site. The consideration of SCFs in the local geometry proved to be crucial for the estimation of the fatigue life of components. Using the traditional approach with no SCF applied and assuming that the corrosion protective system remains fully functional for the full service life of the turbine, the fatigue life was estimated to be 30.45 years. However, when considering the geometric effects of the ring flange, the fatigue life was reduced by 19.3 %, yielding a more realistic estimate of 24.57 years. This result demonstrates the influence of the stress concentrations introduced by the internally bolted ring flange. Such effects give rise to substantial reductions in the turbine tower's projected fatigue life, emphasising the significant influence of the flange on the structural lifespan of the turbine and highlighting the importance of considering these effects in fatigue life assessments.

In addition to geometric stress concentrations, material degradation mechanisms such as corrosion can further compromise fatigue performance. To assess this, the effects of corrosion were investigated by comparing the lifespan of the wind turbine considering various levels of corrosion protection. For a realistic scenario in which the corrosion protection fails after just five years, the wind turbine's lifespan is reduced to just 13.39 years. This significant reduction of more than 45 % in expected lifespan highlights the critical importance of incorporating corrosion effects into structural assessments and implementing effective protection strategies to ensure long-term reliability.

7. Limitations and future works

The fatigue assessment framework developed in this work follows the procedures outlined in IEC 61,400 International Electrotechnical Commission (2019) and incorporates site-specific wind and wave conditions. Nevertheless, several limitations should be noted. First, the butt weld is assumed to be perfectly aligned and the tower sections perfectly circular, which may not reflect real-world fabrication tolerances. Second, corrosion wastage is assumed to progress linearly, simplifying the complex, time-varying nature of real corrosion processes. Third, the fatigue analysis is restricted to DLC 1.2, representing normal operating conditions. As a result, additional fatigue loading contributions from start-up, shut-down, idling, and storm conditions are not captured. Finally, wind and wave conditions are assumed to be fully aligned, and potential misalignment effects are not considered.

To advance this work, future studies should refine the treatment of corrosion. In the present study, corrosion was modelled using the conventional approach of uniform, linear material loss over time. However, further refinement could be achieved by implementing non-uniform corrosion rates and investigating localised corrosion modelling strategies, such as pitting corrosion models.

Future works could additionally address the limitations regarding the loading assumptions by exploring the influence of wind–wave misalignment on fatigue damage accumulation. Investigating the effects of misaligned loading would provide greater confidence in fatigue assessments by ensuring that a broader range of dynamic scenarios are considered, including those that may give rise to potential instabilities in the turbine's response. However, accounting for misaligned wind and wave loading significantly increases the number of required simulations, resulting in substantial computational demands. To address this challenge, machine learning approaches could be employed to reduce computational effort. The integration of such techniques would not only accelerate fatigue analyses but also enable a broader exploration of key variables. In particular, such models could be used to explore the use of advanced control devices and operational strategies to provide effective pathways to mitigate fatigue loading and extend turbine life beyond the required 20-year design threshold.

CRediT authorship contribution statement

James McAuliffe: Writing – original draft, Visualization, Software, Methodology, Investigation, Formal analysis, Data curation, Conceptualization; **Brian Broderick:** Writing – review & editing, Supervision, Methodology; **Breiffni Fitzgerald:** Writing – review & editing, Supervision, Software, Methodology, Investigation, Funding acquisition, Conceptualization.

Declaration of competing interest

The authors declare that they have no known competing financial interests or personal relationships that could have appeared to influence the work reported in this paper.

Acknowledgment

The Funding for this research was provided by the Sustainable Energy Authority of Ireland (SEAI) under the WindLEDeRR project, grant number RDD 601.

References

Abaqus, G., 2011. Abaqus 6.11. Dassault Systemes Simulia Corporation, Providence, RI, USA, 3.

Abbas, N., Zalkind, D., Pao, L., Wright, A., 2021. A reference open-source controller for fixed and floating offshore wind turbines. Wind Energy Sci. Discuss. 2021, 1–33. https://wes.copernicus.org/preprints/wes-2021-19/. https://doi.org/10.5194/wes-2021-19

Adasooriya, N.D., Hemmingsen, T., Pavlou, D., 2017. Fatigue strength degradation of metals in corrosive environments. In: IOP Conference Series: Materials Science and Engineering. Vol. 276. IOP Publishing, p. 012039.

Adasooriya, N.D., Pavlou, D., Hemmingsen, T., 2020. Fatigue strength degradation of corroded structural details: a formula for s-n curve. Fatig. Fract. Eng. Mater. Struct. 43 (4), 721–733.

Baisthakur, S., Fitzgerald, B., 2024. Physics-informed neural network surrogate model for bypassing blade element momentum theory in wind turbine aerodynamic load estimation. Renew. Energy , 120122.

Baisthakur, S., Fitzgerald, B., 2025. Multi-task learning long short-term memory model to emulate wind turbine blade dynamics. Wind Energy Sci. 10 (9), 1979–2004.

Bak, C., Zahle, F., Bitsche, R., Kim, T., Yde, A., Henriksen, L.C., Hansen, M.H., Blasques, J. P. A.A., Gaunaa, M., Natarajan, A., 2013. The DTU 10-MW reference wind turbine. In: Danish Wind Power Research 2013.

Boudounit, H., Tarfaoui, M., Saifaoui, D., 2023. Fatigue analysis of wind turbine composite blade using finite element method. Wind Eng. 47 (3), 706–721.

Chen, Y., Wu, D., Dai, K., Gao, W., 2022. A numerically efficient framework in failure mode evaluation of a wind turbine tower under cyclones. Marine Struct. 86, 103303.

DNV, 2016. Recommended practice DNVGL-RP-0416 corrosion protection for wind turbines. DET NORSK VERITAS: Oslo, Norway.

DNV, 2022. Bladed Theory Manual, Version 4.13. Bristol, UK. https://myworkspace.dnv.com/knowledge-centre/bladed.

DNV, G.L., 2019. DNV-RP-C203: Fatigue Design of Offshore Steel Structures. Technical Report 2019/A2 Edition. DNV GL. https://www.dnv.com/energy/standards-guidelines/dnv-rp-c203-fatigue-design-of-offshore-steel-structures/.

Do, T.Q., van de Lindt, J.W., Mahmoud, H., 2015. Fatigue life fragilities and performance-based design of wind turbine tower base connections. J. Struct. Eng. 141 (7), 04014183.

Dong, W., Moan, T., Gao, Z., 2011. Long-term fatigue analysis of multi-planar tubular joints for jacket-type offshore wind turbine in time domain. Eng. Struct. 33 (6), 2002–2014.

Dong, W., Moan, T., Gao, Z., 2012. Fatigue reliability analysis of the jacket support structure for offshore wind turbine considering the effect of corrosion and inspection. Reliab. Eng. Syst. Safe. 106, 11–27.

Efthymiou, M., 1988. Development of SCF formulae and generalised influence functions for use in fatigue analysis.

Fitzgerald, B., Basu, B., 2016. Structural control of wind turbines with soil structure interaction included. Eng. Struct. 111, 131–151.

Fu, B., Zhao, J., Li, B., Yao, J., Teifouet, A. R.M., Sun, L., Wang, Z., 2020. Fatigue reliability analysis of wind turbine tower under random wind load. Struct. Safe. 87, 101982.

Gaertner, E., Rinker, J., Sethuraman, L., Zahle, F., Anderson, B., Barter, G., Abbas, N., Meng, F., Bortolotti, P., Skrzypinski, W., Scott, G., Feil, R., Bredmose, H., Dykes, K., Sheilds, M., Allen, C., Viselli, A., 2020a. Definition of the IEA 15-Megawatt Offshore Reference Wind Turbine. Technical Report. International Energy Agency. https://www.nrel.gov/docs/fy20osti/75698.pdf.

Gaertner, E., Rinker, J., Sethuraman, L., Zahle, F., Anderson, B., Barter, G.E., Abbas, N.J., Meng, F., Bortolotti, P., Skrzypinski, W., et al., 2020b. IEA wind TCP task 37: definition of the IEA 15-megawatt offshore reference wind turbine. Technical Report. National Renewable Energy Lab.(NREL), Golden, CO (United States).

Hayman, G.J., Buhl Jr, , M., 2012. Mlife Users Guide for Version 1.00. National Renewable Energy Laboratory, Golden, CO 74 (75), 112.

Hegseth, J.M., Bachynski, E.E., Leira, B.J., 2021. Effect of environmental modelling and inspection strategy on the optimal design of floating wind turbines. Reliab. Eng. Syst. Safe. 214, 107706.

Hsu, Y., Wu, W.-F., Chang, Y.-C., 2014. Reliability analysis of wind turbine towers. Proced. Eng. 79, 218–224.

Hu, W., Choi, K.K., Zhupanska, O., Buchholz, J. H.J., 2016. Integrating variable wind load, aerodynamic, and structural analyses towards accurate fatigue life prediction in composite wind turbine blades. Struct. Multidiscipl. Optimiz. 53, 375–394.

Hu, Y., Baniotopoulos, C., Yang, J., 2014. Effect of internal stiffening rings and wall thickness on the structural response of steel wind turbine towers. Eng. Struct. 81, 148–161.

Huo, T., Tong, L., 2020. An approach to wind-induced fatigue analysis of wind turbine tubular towers. J. Construct. Steel Res. 166, 105917.

International Electrotechnical Commission. IEC 61400-3-1, Wind turbines-Part 3-1: Design requirements for offshore wind turbines, Committee Draft. sl: IEC, 2014. Technical Report. IEC 61400-3-1.

International Electrotechnical Commission, 2019. IEC 61400-1. Wind Energy Generation Systems-Part 1: Design Requirements. International Electrotechnical Commission, Geneva, Switzerland.

International Electrotechnical Commission, 2020. IEC 61400-6: Wind Energy Generation System - Part 6: Tower and Foundation Design Requirements. International Electrotechnical Commission.

Jonkman, B., Platt, A., Mudafort, R.M., Branlard, E., Sprague, M., Ross, H., Jonkman, J., Hayman, G., Slaughter, D., Hall, M., et al., 2024. OpenFAST/openfast: v3. 5.2. https://doi.org/Zenodohttps://doi.org/10.5281/zenodo 10530537.

Jonkman, B.J., 2009. TurbSim user's guide: Version 1.50. Technical Report. National Renewable Energy Lab.(NREL), Golden, CO (United States).

Jonkman, J.M., Buhl Jr, , M.L., 2005. Fast user's Guide. National Renewable Energy Laboratory, Golden, CO, Technical Report No. NREL/EL-500-38230.

Kane, T.R., Levinson, D.A., 1985. Dynamics, theory and applications. McGraw Hill.

Kensche, C.W., 2006. Fatigue of composites for wind turbines. Int. J. Fatig. 28 (10), 1363–1374.

Larsen, T.J., Hansen, A.M., 2007. How 2 HAWC2, the User's Manual. Risø National Laboratory.

Li, B., Shi, H., Rong, K., Geng, W., Wu, Y., 2023. Fatigue life analysis of offshore wind turbine under the combined wind and wave loadings considering full-directional wind inflow. Ocean Eng. 281, 114719.

Li, T., Yang, Q., Zhang, X., Ma, Y., 2024. Efficient fatigue damage estimation of offshore wind turbine foundation under wind-wave actions. J. Construct. Steel Res. 221, 108903.

Li, Y., Zhang, Y., Wang, W., Li, X., Wang, B., 2022. Influence of corrosion damage on fatigue limit capacities of offshore wind turbine substructure. J. Marine Sci. Eng. 10 (8), 1011.

Lotsberg, I., 2016. Fatigue Design of Marine Structures. Cambridge University Press.

Lotsberg, I., 2025. Derivation of design SN curves for butt welds in support structures for wind turbines. Marine Struct. 102, 103795.

MATLAB, 2018. Version 9.4.0 (R2018a). The MathWorks Inc., Natick, Massachusetts.

McAuliffe, J., Baisthakur, S., Broderick, B., Fitzgerald, B., 2024. Corrosion fatigue analysis of NREL's 15-MW offshore wind turbine with time-varying stress concentration factors. In: Journal of Physics: Conference Series. Vol. 2767. IOP Publishing, p. 062023.

Momber, A.W., 2016. Quantitative performance assessment of corrosion protection systems for offshore wind power transmission platforms. Renew. Energy 94, 314–327.

Morison, J.R., Johnson, J.W., Schaaf, S.A., 1950. The force exerted by surface waves on piles. J. Petrol. Technol. 2 (05), 149–154.

Muskulus, M., Schafhirt, S., 2015. Reliability-based design of wind turbine support structures. In: Proceedings of the Symposium on Reliability of Engineering System, Hangzhou, China. Vol. 1517.

Nispel, A., Ekwaro-Osire, S., Dias, J.P., Cunha Jr, , A., 2021. Uncertainty quantification for fatigue life of offshore wind turbine structure. ASCE-ASME J. Risk Uncert. Eng. Syst., Part B: Mech. Eng. 7 (4), 040901.

Okenyi, V., Bodaghi, M., Siegkas, P., Mansfield, N., Afazov, S., 2023. Stress analyses of high-rated capacity large diameter offshore wind turbines: analytical and numerical analyses of uniform corrosion effects. Proceedings of the Institution of Mechanical Engineers, Part C: Journal of Mechanical Engineering Science, 09544062231208551.

Peng, M., Liu, M., Gu, S., Nie, S., 2023. Multiaxial fatigue analysis of jacket-type offshore wind turbine based on multi-scale finite element model. Materials 16 (12), 4383.

Petroleum, I., 2007. Natural Gas Industries-Fixed Steel Offshore Structures (ISO 19902). International Organization for Standardization (ISO): Geneva, Switzerland.

Pierson Jr, W.J., Moskowitz, L., 1964. A proposed spectral form for fully developed wind seas based on the similarity theory of SA kitaigorodskii. J. Geophys. Res. 69 (24), 5181–5190.

Pilkey, W.D., Pilkey, D.F., Bi, Z., 2020. Peterson's Stress Concentration Factors. John Wiley & Sons.

Pu, Y., Dong, Y., Fitzgerald, B., 2025. Integrated IPC-TMDI control for mitigating fatigue in floating offshore wind turbines under misaligned wind-wave loading. Ocean Eng. 333, 121491.

Radaj, D., Sonsino, C.M., Fricke, W., 2006. Fatigue Assessment of Welded Joints by Local Approaches. Woodhead publishing.

Ren, C., Aoues, Y., Lemosse, D., De Cursi, E.S., 2023. Reliability assessment of an offshore wind turbine jacket under one ultimate limit state considering stress concentration with active learning approaches. Ocean Eng. 281, 114657.

Saenz-Aguirre, A., Ulazia, A., Ibarra-Berastegi, G., Saenz, J., 2022. Floating wind turbine energy and fatigue loads estimation according to climate period scaled wind and waves. Energy Convers. Manage. 271, 116303.

Sajeer, M.M., Mitra, A., Chakraborty, A., 2020. Spinning finite element analysis of longitudinally stiffened horizontal axis wind turbine blade for fatigue life enhancement. Mech. Syst. Signal Process. 145, 106924.

Sarkar, S., Chen, L., Fitzgerald, B., Basu, B., 2020. Multi-resolution wavelet pitch controller for spar-type floating offshore wind turbines including wave-current interactions. J. Sound Vibrat., 115170.

Sarkar, S., Fitzgerald, B., 2020. Vibration control of spar-type floating offshore wind turbine towers using a tuned mass-damper-inerter. Struct. Control Health Monitor. 27 (1), e2471.

Sarkar, S., Fitzgerald, B., 2021. Use of kane's method for multi-body dynamic modelling and control of spar-type floating offshore wind turbines. Energies 14 (20), 6635.

Seidel, M., 2020. Analytical calculation of stress concentrations at welded flange necks. Stahlbau 89 (6), 551–560.

Song, Y., Sun, T., Zhang, Z., 2023. Fatigue reliability analysis of floating offshore wind turbines considering the uncertainty due to finite sampling of load conditions. Renew. Energy 212, 570–588.

Sørum, S.H., Katsikogiannis, G., Bachynski-Polić, E.E., Amdahl, J., Page, A.M., Klinkvort, R.T., 2022. Fatigue design sensitivities of large monopile offshore wind turbines. Wind Energy 25 (10), 1684–1709.

Stavridou, N., Efthymiou, E., Baniotopoulos, C.C., 2015. Welded connections of wind turbine towers under fatigue loading: finite element analysis and comparative study. Am. J. Eng. Appl. Sci. 8 (4), 489–503.

Stewart, G.M., Robertson, A., Jonkman, J., Lackner, M.A., 2016. The creation of a comprehensive metocean data set for offshore wind turbine simulations. Wind Energy 19 (6), 1151–1159.

Tao, T., Yang, Y., Yang, T., Liu, S., Guo, X., Wang, H., Liu, Z., Chen, W., Liang, C., Long, K., et al., 2024. Time-domain fatigue damage assessment for wind turbine tower bolts under yaw optimization control at offshore wind farm. Ocean Eng. 303, 117706.

Velarde, J., Kramhøft, C., Sørensen, J.D., Zorzi, G., 2020. Fatigue reliability of large monopiles for offshore wind turbines. Int. J. Fatig. 134, 105487.
Wang, H., Barthelmie, R.J., Pryor, S.C., Kim, H.G., 2014. A new turbulence model for offshore wind turbine standards. Wind Energy 17 (10), 1587–1604.
Wang, S., Moan, T., Jiang, Z., 2022. Influence of variability and uncertainty of wind and waves on fatigue damage of a floating wind turbine drivetrain. Renew. Energy 181, 870–897.
Weijtjens, W., Stang, A., Devriendt, C., Schaumann, P., 2021. Bolted ring flanges in offshore-wind support structures-in-situ validation of load-transfer behaviour. J. Construct. Steel Res. 176, 106361.
Yang, H., Zhu, Y., Lu, Q., Zhang, J., 2015. Dynamic reliability based design optimization of the tripod sub-structure of offshore wind turbines. Renew. Energy 78, 16–25.
Yeter, B., Garbatov, Y., Guedes Soares, C., 2014a. Fatigue damage analysis of a fixed offshore wind turbine supporting structure. Developments in Maritime Transportation and Exploitation of Sea Resources. London, UK: Taylor & Francis Group, 415–424.
Yeter, B., Garbatov, Y., Guedes Soares, C., 2014b. Spectral fatigue assessment of an offshore wind turbine structure under wave and wind loading. Developments in Maritime Transportation and Exploitation of Sea Resources. London, UK: Taylor & Francis Group , 425–433.
Yeter, B., Garbatov, Y., Soares, C.G., 2016. Evaluation of fatigue damage model predictions for fixed offshore wind turbine support structures. Int. J. Fatig. 87, 71–80.
Zhang, C., Chen, H.-P., Huang, T.-L., 2018. Fatigue damage assessment of wind turbine composite blades using corrected blade element momentum theory. Measurement 129, 102–111.
Zhang, J., Heng, J., Dong, Y., Baniotopoulos, C., Yang, Q., 2024a. Coupling multi-physics models to corrosion fatigue prognosis of high-strength bolts in floating offshore wind turbine towers. Eng. Struct. 301, 117309.
Zhang, X.-L., Zhang, B.-j., Wang, D., Xu, C.-s., 2024b. Fatigue damage analysis method of offshore wind turbine foundation. Ocean Eng. 302, 117618.
Zhu, D., Ding, Z., Huang, X., Li, X., 2023. Probabilistic modeling for long-term fatigue reliability of wind turbines based on markov model and subset simulation. Int. J. Fatig. 173, 107685.
Zwick, D., Muskulus, M., 2016. Simplified fatigue load assessment in offshore wind turbine structural analysis. Wind Energy (2), 265–278.